Electroless Nickel Plating of Electropolished and Chempolished Additively Manufactured (AM) Steel Components in Various Surface Orientations

Wondwosen Demisse[1], Pablo Sanchez[1], Daniel Fulford[1], Lucas Rice[2], Kate L. Klein[1], Pawan Tyagi[1*]

[1]Mechanical Engineering, University of the District of Columbia Washington, DC, 20008, USA

[2]Kansas City Nuclear Security Campus, Honeywell Federal Manufacturing & Technologies, LLC, Kansas City, MO, 64147, USA

Corresponding Author Email: ptyagi@udc.edu

Abstract

Electroless coating brings the advantage of providing films on the complex geometry of additively manufactured components. However, there is a knowledge gap about the impact of AM part surface and postprocessing parameters on the quality of electroless coating. This study explores the application of three solution-based surface finishing techniques on the microstructure and surface hardness of additively manufactured stainless steel components coated with electroless nickel films. Given that AM techniques for metal parts often yield surfaces with inherently rough textures and differences in properties along the different planes, we investigated their relationship with nickel coating. To mitigate the impact of surface irregularities on electroless nickel coating quality, this research evaluated the effectiveness of chemical polishing (CP) and Electropolishing (EP) as post-processing treatments for AM stainless steel. Characterization of the treated samples was conducted using the analytical Digital Microscope, Scanning Electron Microscope (SEM), and scratch tester. Additionally, the study incorporated an instant segmentation machine learning algorithm to overcome image analysis challenges. The findings indicate that EP and CP significantly improve surface smoothness, decreasing the arithmetical mean height (Ra) by as much as 4 µm and 10 µm, respectively. Furthermore, the nickel-coated AM samples demonstrated an enhancement in scratch resistance, exhibiting up to a two-fold increase in surface hardness compared to their as-built counterparts. Taguchi design of the experiment was applied to investigate the effect of process parameters. This study provides insights for developing improved surface quality and acquiring new properties via the coating process to make AM parts suitable for challenging environments and novel applications.

Keywords: Additive manufacturing, electroless nickel, scratch test, 3D printing, Laser metal sintering.

1. INTRODUCTION

Additive manufacturing (AM) has brought a significant paradigm shift in the realm of product design and manufacturing [1-4]. AM has substantially enhanced the efficiency of producing intricate metal components. However, as produced AM components remain susceptible to various issues, including wear [5-7], corrosion [8-11], fatigue [12-14], normal stress [15-17], and shear [18-21]. AM components are needed to exhibit qualities such as high toughness, durability, and corrosion resistance. However, achieving the desired mechanical properties within a single material or production process presents a formidable challenge. Some materials may demonstrate exceptional corrosion resistance but simultaneously exhibit heightened susceptibility to mechanical stress, whereas others may possess remarkable deformation resistance but may prove unsuitable for utilization in acidic or saline

environments [22, 23]. It is widely recognized that the surface quality of a manufactured component has a direct bearing on factors such as wear, corrosion, and the initiation of cracks [24]. In cases where a component's surface finish is suboptimal, the likelihood of failure is considerably elevated [25]. Consequently, various post-processing techniques, including heat treatment, chemical treatment, spray coating, electroplating, and electroless plating, are extensively employed to ameliorate surface integrity and mitigate corrosion-related concerns [26, 27]. It is a common observation that the as-produced surfaces of AM parts often fall short of the desired quality standards, necessitating post-processing interventions [28-30].

Electropolishing, also referred to as electrochemical polishing (Fig. 1a), is a technique primarily used on metals such as stainless steel and aluminum for reducing surface roughness [31]. The process involves submerging the metal component in an electrolyte, typically with an acidic composition. After that, an electrical current is applied, with the metal component acting as the anode. This initiates an electrochemical reaction that selectively eliminates a thin layer of material from the surface of the metal. As a result, numerous advantages are achieved [32]. Electropolishing effectively smooths the surface by eliminating scratches, imperfections, and microscopic peaks. It also excels in eliminating contaminants and embedded particles, thereby enhancing the cleanliness of the material. Furthermore, electropolishing contributes to improved corrosion resistance and significantly enhances surface brightness and reflectivity [33]. However, electropolishing is not possible for very intricate shapes involving difficult-to-access surface areas. For such a situation, chempolishing can be adopted since it does not require typical counter electrode proximity to the target surface and electricity flow necessary in Electropolishing (Fig.1a). Our group has implemented chempolishing as the effective surface improvement method for the complex-shaped AM steel components[34] and also compared the advantages of this method with respect to electropolishing [25]. Chempolishing (Fig. 1b) is a chemical polishing technique that exhibits versatility in its application, catering to both metal and non-metal materials. This process entails immersing the component in a chemical bath specifically tailored for the material at hand [35]. The chemical solution selectively interacts with the surface, removing microscopic irregularities and asperities [36]. Chempolishing achieves surface uniformity and smoothness, making it highly effective in eliminating surface contaminants, oxides, and stains. It is a preferred method for enhancing the overall appearance of the material, offering an appealing and polished finish. Additionally, chempolishing can also contribute to improved corrosion resistance in certain cases [37]. Further advancements in the post-processing of chempolished and electropolished AM components are possible through the integration of electroless coating. However, there is a knowledge gap in the literature regarding the effects of electroless coating on chempolished and electropolished AM steel components.

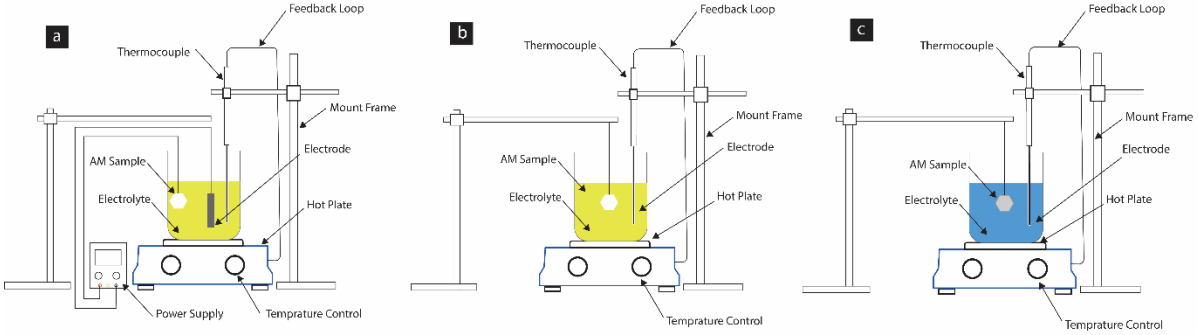

Fig 1. Schematics of experimental set up for (a) Electropolishing, (b) Chempolishing, and (c) electroless nickel plating of any sample.

Electroless plating offers excellent opportunities to bring a wide range of new properties not available for metal and alloys after additive manufacturing. Similar to chempolishing, electroless plating can occur without requiring complex instrumentation and is relatively unaffected by the AM part geometry. Electroless nickel plating is a very popular and successful method for improving surface wear resistance and corrosion protection. Electroless nickel plating (Fig. 1c), a highly versatile and controlled process, plays a pivotal role in surface modification and engineering applications [38]. Unlike electroplating, it does not necessitate an external electrical current for metal deposition, rendering it a self-catalytic process. In this method, a carefully formulated aqueous solution comprising a reducing agent and a source of nickel ions is utilized to deposit a uniform layer of nickel onto the surface of a substrate, typically composed of metals like steel, aluminum, or copper [39, 40]. The reduction reaction occurring on the substrate surface facilitates the controlled and precise deposition of nickel, leading to enhanced surface properties such as wear resistance, corrosion protection, and improved hardness. Electroless nickel plating finds wide-ranging utilization in industries encompassing aerospace, automotive, electronics, and engineering, owing to its ability to confer desirable material enhancements and precise coating thickness control [41, 42]. According to the available literature, there are gaps in understanding of how surface orientation and solution-based electropolishing and chempolishing post-processing methods affect the electroless nickel coating process for additively manufactured (AM) steel components.

In the present study, we have investigated three surface finishing methodologies to enhance the surface quality of additively manufactured surfaces (Fig. 1). Our investigation predominantly centers on the application of chemical-based techniques for reducing surface roughness in additively manufactured stainless steel specimens. The selection of chemical etching methodologies stems from their effectiveness in reducing surface roughness in concealed areas. We utilized electropolishing and chempolishing processes to smooth surfaces. Additionally, we expound upon our procedure for the generation of a protective coating on the chemically refined surfaces of the specimens. Our chosen approach involves the application of electroless nickel coatings to additively manufactured stainless steel samples. This paper provides a comprehensive exposition of the experimental procedures employed in obtaining EP, CP, and electroless nickel coatings, accompanied by the application of machine learning instance segmentation for the analysis of microscopic and scanning electron microscopy (SEM) images.

2. METHODOLOGY

2.1 Sample Material

The sample material chosen for this study is a molybdenum-alloyed austenitic steel, specifically stainless steel 316. Its composition primarily comprises iron, chromium, nickel, and molybdenum, with mass percentages typically falling within the range of 55-60% iron, 17-19% chromium, 13-15% nickel, 2-3% molybdenum, 6-8% carbon, along with trace amounts of other elements such as manganese and silicon (Fig. 2). The raw material powder, used in the experimentation, is spherical in shape and has a nominal particle size of 25 ± 15 µm. The production of stainless-steel powder is achieved through the atomization process, a well-established technique in powder metallurgy. Atomization entails the initial melting of the stainless steel 316 alloy, followed by subjecting it to high-pressure gas or water

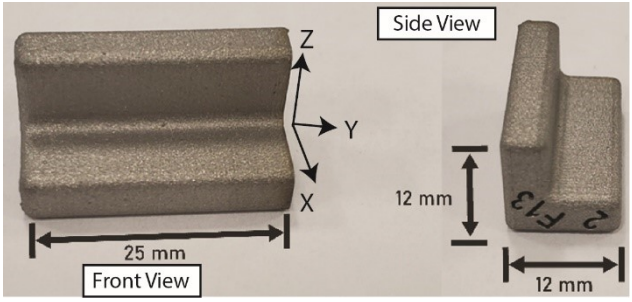

Fig 2. L-shaped stainless steel AM samples.

jets to disintegrate the molten metal into fine droplets. These droplets subsequently undergo rapid solidification, resulting in the formation of spherical particles during the cooling phase.

2.2 Sample fabrication

The specimens are fabricated using the EOS M280 laser sintering-based metal 3D printer housed within the facilities of the Kansas City National Security Campus. The optimization of the 3D printing process for Stainless Steel 316L samples with the EOS M280 laser sintering-based metal 3D printer necessitates meticulous attention to crucial parameters. The process of fine-tuning involves the establishment of a layer thickness of 40 microns, a laser power of 400 Watts, and a scanning speed of 7 m/s. Furthermore, the Powder Bed and Build Chamber Temperature maintained at 40 degrees Celsius ensures the creation of optimal sintering conditions. A nitrogen gas atmosphere is employed to prevent oxidation during the printing process and enhance the final product's quality. The implementation of these parameters guarantees the attainment of high-quality results in the 3D printing of stainless-steel specimens.

2.3 Sample preparation

The sample preparation involved a series of sequential procedures designed to ensure the removal of various impurities and contaminants from the surface of the test specimens (Fig. 3). These contaminants typically encompass substances such as greases, oils, organic and inorganic compounds, tarnish, light rust, fingerprints, and oxides. Initially, the samples are subjected to a 3-minute sonication process in acetone, a solvent well-suited for dissolving greases, oils, resins, inks, permanent markers, adhesives, and paints. Subsequently, the samples undergo a thorough rinse with distilled water and are dried using a blower. Following this preliminary cleaning, the specimens are subjected to a further 3-minute sonication step, utilizing 99% isopropyl alcohol (IPA), in an ultrasonic sonicator. This stage is instrumental in dissolving any remaining impurities on the sample surface.

Following the IPA sonication, the next phases encompass intermediate-alkaline cleaning and electro-cleaning. Intermediate-alkaline cleaning is accomplished by immersing the samples in a sodium hypochlorite solution at 82 °C for a brief duration of 2 minutes. This process serves to eliminate residual solvents and oils that may have been loosened during the initial pre-cleaning phase.

Subsequent to intermediate-alkaline cleaning, the samples undergo a thorough rinse, drying, and electro-cleaning (EC). EC is an electrochemical process that utilizes an alkaline electrolyte and direct current (DC). In our experimental setup, a ready-to-use solution from Krohn Industrial Inc. was employed, maintaining the bath temperature at 50°C and applying a voltage of 10V for a duration of one and a half minutes between the sample and titanium anode. Krohn Industrial Inc.'s electro-cleaning solution is designed to prepare steel surfaces for electroless plating by effectively removing contaminants and oxides. The solution typically contains a blend of alkalis and surfactants, which function to clean and etch the steel substrate. It operates at a pH range of 10 to 13. The electrocleaning process involves applying a voltage to the solution, facilitating the removal of organic and inorganic residues from the steel surface. During electro-cleaning, the titanium anode was positioned within the tank. The steel components being cleaned serve the role of cathode and are connected to the anode via a power supply. These anode and cathode are immersed in the electro-cleaning solution. This electro-cleaning operation results in the formation of an oxide layer on the sample surface, necessitating a subsequent acid dip in 3M HCL for 40 seconds to remove the oxide layer and neutralize the sample. This pre-treatment ensures optimal adhesion and performance of the subsequent electroless plating.

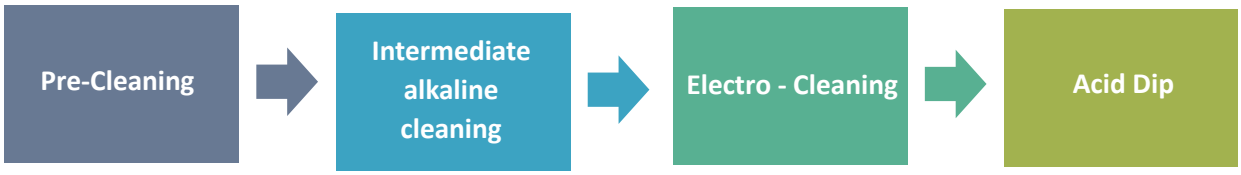

Fig 3. Standard cleaning process steps

The electropolishing method hinges on the use of highly concentrated acidic electrolytes, continually dissolving the sample throughout the electropolishing procedure. In electropolishing, the electrolyte comprises a mixture of 70% phosphoric acid and 30% sulfuric acid by volume, with the preferred operational temperature sustained at 75°C. The sample is electrically connected to a power source along with the lead electrode, whereby the negative terminal is linked to the electrode (cathode), and the positive terminal is associated with the sample (anode). A current density of 70 A/dm^2 is diligently applied over the course of 30 minutes during the electropolishing process. An alkaline solution is judiciously employed to neutralize the sample post-electropolishing. To execute the chempolishing (CP) procedure, a highly concentrated acidic solution is employed as an electrolyte, serving the purpose of dissolving the areas of high-stress concentration and crack nucleation present on the submerged sample within the chemical bath. Notably, this process is electroless, with surface refinement occurring subsequent to the cleaning phase. The chemical bath, constituting a composition of 10-30% phosphoric acid, 1-10% hydrochloric acid, 1-10% nitric acid, and 1-10% proprietary surfactants, is an important component of the chempolishing regimen. It is of paramount importance to rigorously maintain the bath temperature at a constant 75°C throughout the procedure, as deviations in temperature could lead to contamination of the chemical bath. Furthermore, agitation emerges as a critical element in the chempolishing protocol, effectively dispersing localized heat generated during the electropolishing phase. In the experiments that were conducted, agitation was executed through the utilization of a 20 mm magnetic stirrer set at 200 rpm. Following a 30-minute dissolution period, the samples were meticulously rinsed in distilled water.

2.4 Electroless nickel plating

In the domain of electroless nickel plating, it is customary to employ three distinct types of solutions. The crucial determinant in the deposition of nickel lies in the concentration of phosphorus within these solutions. In the scope of our specific investigation, we utilized electroless nickel plating solutions classified into three categories: low phosphorus (ONE PLATE 3001), mid phosphorus (ONE PLATE 1001), and high phosphorus (ONE PLATE 2001) (Table 1). These solutions were procured from Plating International Inc., which was recognized for their stability and characterized by pH values within the range of 5 to 6. It is imperative to ensure the pristine condition of the sample prior to commencing the deposition process, as any surface impurities may detrimentally affect the quality of deposition and impede the adhesion of the nickel coating. Therefore, a prerequisite is to thoroughly clean the substrate, free from any extraneous debris, oils, greases, or oxide layers. So, the sample must pass through the standard cleaning process. Once this preparatory phase is concluded, the sample is ready to undergo activation.

Table 1. Electroless nickel solution content and properties acquired from Plating International Inc.

Plating Solution	Trade name	pH	Phosphurs Content (by weight)	Operation temperature (°C)	Plating rate (micro/Hr)
Low Phosphorus	ONE PLATE 3001	5.8	3 to 5%	90	20
Mid Phosphorus	ONE PLATE 1001	5.8	6 to 9%	90	17
High Phosphorus	ONE PLATE 2001	5.0	10 to 13%	85	10

Certain metals necessitate surface activation to guarantee optimal adhesion for subsequent plating [43, 44]. In our experiment, the sample underwent activation through immersion in a Woods nickel strike solution while being subjected to a direct current (DC) of 5V for a duration of 30 seconds. The plating procedure is conducted immediately after activation. The maintenance of an ideal temperature is of paramount importance during the electroless plating process, as any slight deviation in temperature could trigger an exothermic reaction with the potential to compromise the integrity of the samples. The recommended temperature for the bath solution in the case of low and medium phosphorus is 90°C, while for high phosphorus solutions, it is set at 85°C. The deposition time allocated for all samples was set at 30 minutes.

Table 2. L9 Taguchi design of experiment (TDOE)

DOE	Phosphorus Content	Surface Finish	Orientation	Temperature
1	High	Elec-Polishing	XY Plane	T + 5
2	High	Chempolishing	YZ Plane	T
3	High	As-Built	XZ Plane	T - 5
4	Mid	Elec- Polishing	YZ Plane	T - 5
5	Mid	Chempolishing	XZ Plane	T + 5
6	Mid	As-Built	XY Plane	T
7	Low	Elec- Polishing	XZ Plane	T
8	Low	Chem- Polishing	XY Plane	T - 5
9	Low	As-Built	YZ Plane	T + 5

2.5 Taguchi Design of Experiment (TDOE)

In the course of our experimental investigation, we employed a Taguchi Design of Experiments (TDOE) methodology, which encompasses a series of controlled experiments characterized by four parameters, each exhibiting three distinct levels. The first parameter under scrutiny pertains to the concentration of phosphorus within the electroless nickel solution, with categorizations ranging from low, medium, and high levels. The second parameter centers around the type of surface finishing applied to ameliorate surface roughness, namely Electropolishing (EP), Chempolishing (CP), and the inherent as-built surfaces. The third parameter addresses the configuration of the 3D part coordinate plane, which significantly influences the surface characteristics resulting from the selective laser melting process. The core objective of our study lies in elucidating the responses of different plane surfaces to the deposition process. Finally, the fourth parameter revolves around the temperature of the nickel solution, which necessitates an optimal bath temperature tailored to each level. Our aim is to discern the manner in which the nickel

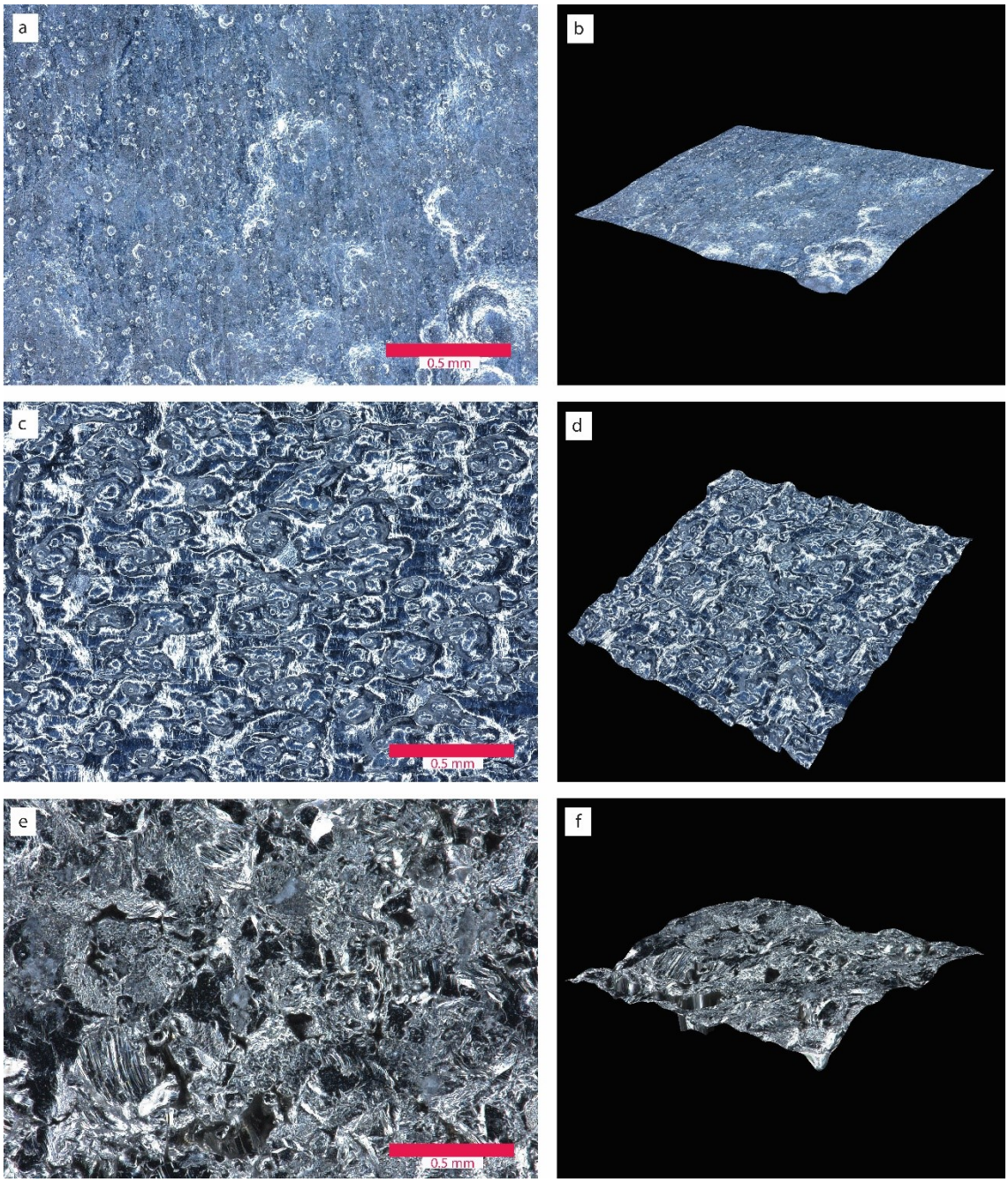

Fig 4. Microscopic imagery for (a) Top view - electropolishing, (b) Isometric view - electropolishing, (c) Top view - chempolishing, (d) Isometric view - chempolishing, (e) Top view – as built, (f) Isometric view - as built.

solution reacts to temperature fluctuations relative to the established optimum temperature. To optimize the quality of experiments while concurrently streamlining the allocation of time and resources, we have adopted a strategic approach encompassing a temperature range spanning 5°C both below and above the defined optimum temperature (Table 2). Through the judicious application of TDOE orthogonal arrays, we have effectively curtailed the number of requisite experiments to a total of nine trials (Table 2). This methodological approach not only ensures the efficient utilization of resources and time but also provides

an in-depth understanding of the effect of different parameters and the correlation among them. It provides an in-depth understanding of the effect of different parameters and their correlation.

3. RESULTS AND DISCUSSION

3.1 Surface roughness characterization after EP, CP, and as-built AM samples were conducted utilizing the SEM (Fig. 4a-f) and KEYENCE Digital Microscope VHX-7000 (Fig. 5). We prepared one sample each for each design of the experiment. The pictorial depiction of key roughness parameters we included in this study is shown in Figure 5a. Ra is the arithmetic average of the absolute values of the surface profile deviations from the mean line, measured over a specific sampling length. It quantifies the average height of the surface irregularities. Rz measures the average height of the roughness profile by calculating the distance between the highest peak and the lowest valley over a specified sampling length. It reflects the peak-to-valley height and provides insight into the overall texture of the surface. RzJIS measures the average peak-to-valley height of the surface profile over a specified length. This value indicates the overall surface roughness by averaging the vertical distances between the highest peaks and the lowest valleys over several sampling lengths. Rp measures the height of the highest peak above the mean line within a given sampling length. It reflects the maximum elevation of the surface profile. Rv measures the depth of the lowest valley below the mean line within a given sampling length. It reflects the maximum depression of the surface profile.

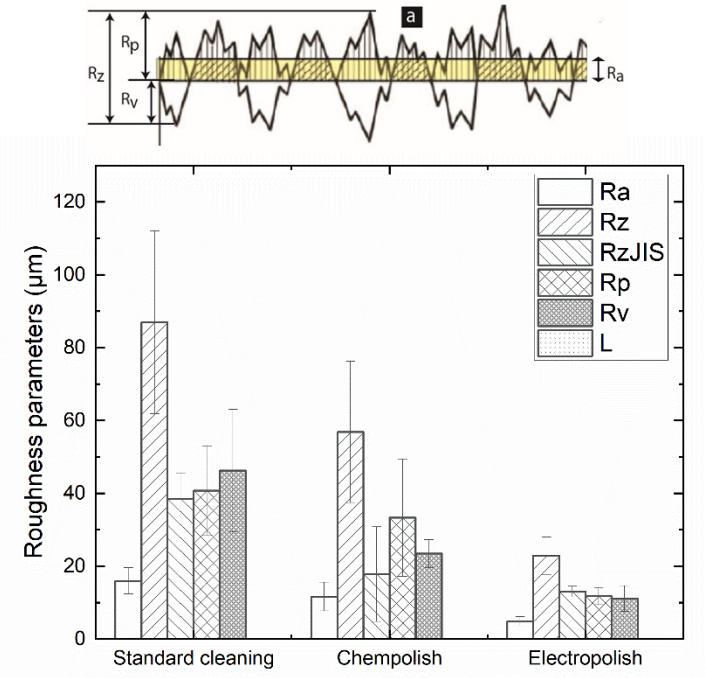

Fig 5. (a) Pictorial description of roughness parameters. (b) Bar chart for different topographical parameters after three surface finishing methods.

Figures 4a and 4b, present the outcomes of the electropolishing surface finishing technique, revealing a substantially flatter topography with diminished hills and peaks. Figure 5 (b) summarizes different roughness parameters for the AM surface after three types of cleaning. The associated surface roughness parameters are: Ra = 4.85 µm, Rz = 22.89 µm, RzJIS = 13.02 µm, Rp = 11.76 µm and Rv = 11.13 µm (Fig. 5b). Figure 4c and 4d, illustrate the surface finish post chempolishing. The corresponding surface roughness measurements are as follows: Ra = 11.65 , Rz = 56.84 µm, RzJIS = 17.79 µm, Rp = 33.33 µm and Rv = 23.50 µm (Fig. 5b). Figure 4e-f, depict the surface topography of the as-built samples. The surface roughness parameters for the as-built specimens are as follows: Ra (arithmetic mean roughness) = 15.95 µm, Rz (the average maximum peak) = 86.99 µm, RzJIS (Ten-point mean roughness) = 38.54 µm, Rp (Maximum profile peak) = 40.73 µm, and Rv (Maximum profile valley depth) = 46.26 µm (Fig. 5b). Figure 4 and 5 suggests that surface topography and roughness changed significantly after chempolishing and electropolishing.

3.2 Surface Roughness Characterization after Nickel Plating

To gain insight into the role of the surface treatment method and different coating parameters, we investigated the 9 specimens prepared as per the Taguchi Design of the experiment scheme (Table 2). Figure 6 shows the topography of different DOE specimens, whereas Figure 7 summarizes the roughness data on each specimen quantitatively. Figure 6a in our study portrays the outcomes of Design of Experiment (DOE) #1, where a specific set of experimental parameters was employed (Table 2). These

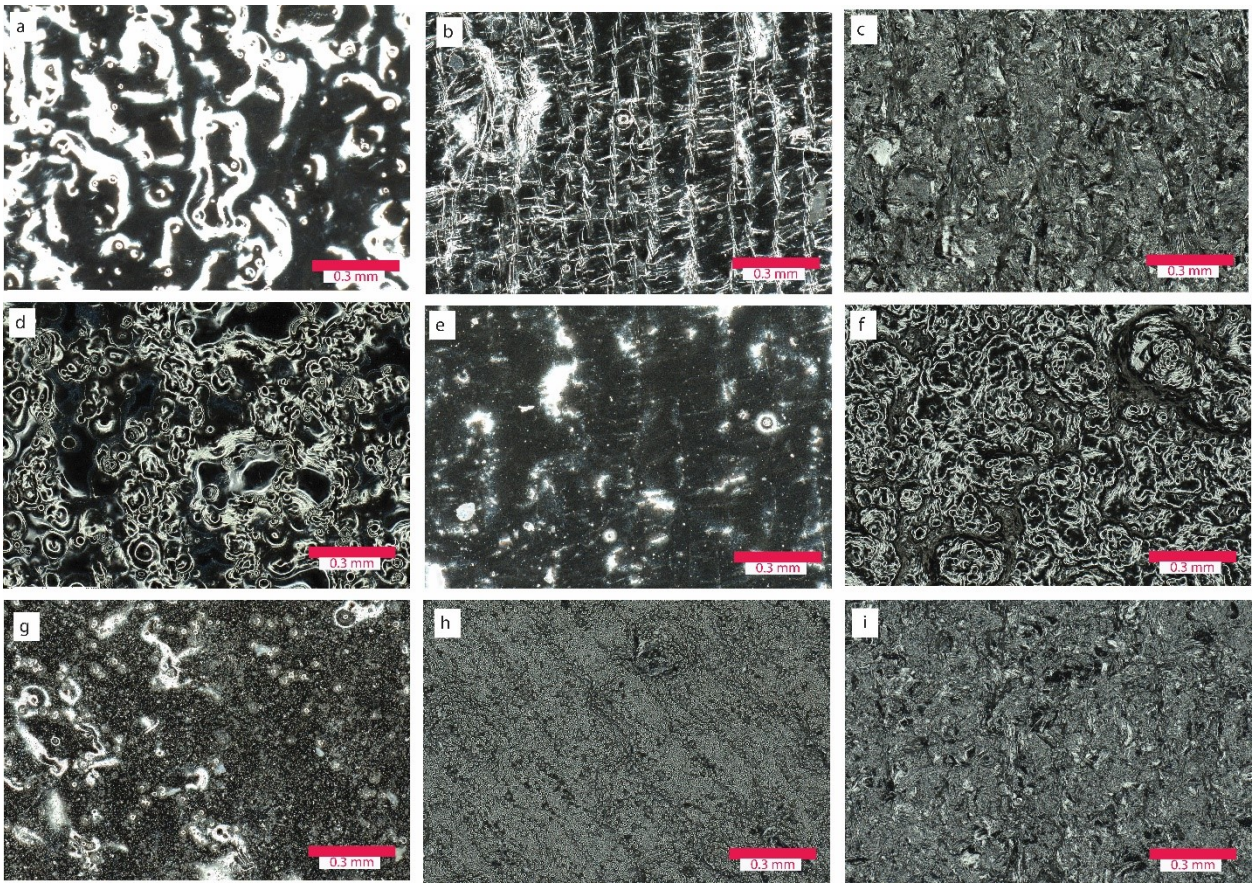

Fig 6. Microscopy imagery for (a) DOE#1, (b) DOE#2, (c) DOE#3, (d) DOE#4, (e) DOE#5, (f) DOE#6, (g) DOE#7, (h) DOE#7, (i) DOE#8, (j) DOE#9

parameters encompassed the utilization of a high phosphorus nickel solution, an electropolished surface finish, orientation within the XY plane, and an elevated temperature exceeding the optimum by 5°C. (Fig.7)Figure 6b, denoting DOE#2, features a distinct combination of experimental parameters involving a high phosphorus nickel solution, chempolished surface finish, alignment along the YZ plane, and an optimal temperature setting (Fig.7). The resultant surface roughness measurements are as follows: Ra = 10.90 µm, Rz = 49.99 µm, RzJIS = 34.61 µm, Rp = 23.1 µm, Rv = 26.89 µm, Rc = 37.03 µm, Rt = 49.99 µm, and Rq = 12.90 µm (Fig.7). In Figure 6c, we present the outcomes of DOE#3, executed with the utilization of a high phosphorus nickel solution, an as-built surface finish, alignment along the XZ plane, and a temperature setting lower than the optimum by 5°C. The measurements of surface roughness revealed the following values: Ra = 15.76 µm, Rz = 70.21 µm, RzJIS = 19.22 µm, Rp = 35.01 µm, Rv = 35.20 µm, Rc = 35.63 µm, Rt = 70.23 µm, and Rq = 18.77µm. Fig 6d, representing DOE#4, comprises parameters involving

a mid-phosphorus nickel solution, an electropolished surface finish, alignment along the YZ plane, and a temperature set lower than the optimum by 5°C. The surface roughness characteristics of this configuration resulted in: Ra = 15.15 µm, Rz = 67.91 µm, RzJIS = 36.42 µm, Rp = 38.38 µm, Rv = 29.53 µm, Rc = 43.58 µm, Rt = 67.94 µm, and Rq = 18.21 µm. Figure 6e, representing DOE#5, describes an experimental framework characterized by using a mid-phosphorus nickel solution, CP surface finish, alignment along the XZ plane, and an elevated temperature surpassing the optimum by 5°C. Surface roughness measurements for this setup yielded the following results: Ra = 14.59 µm, Rz = 73.4 µm, RzJIS = 36.18 µm, Rp = 32.95 µm, Rv = 40.45 µm, Rc = 44.43 µm, Rt = 73.4 µm, and Rq = 17.48 µm. Figure 6f, representative of DOE#6, outlines a specific combination of parameters that incorporates a mid-phosphorus

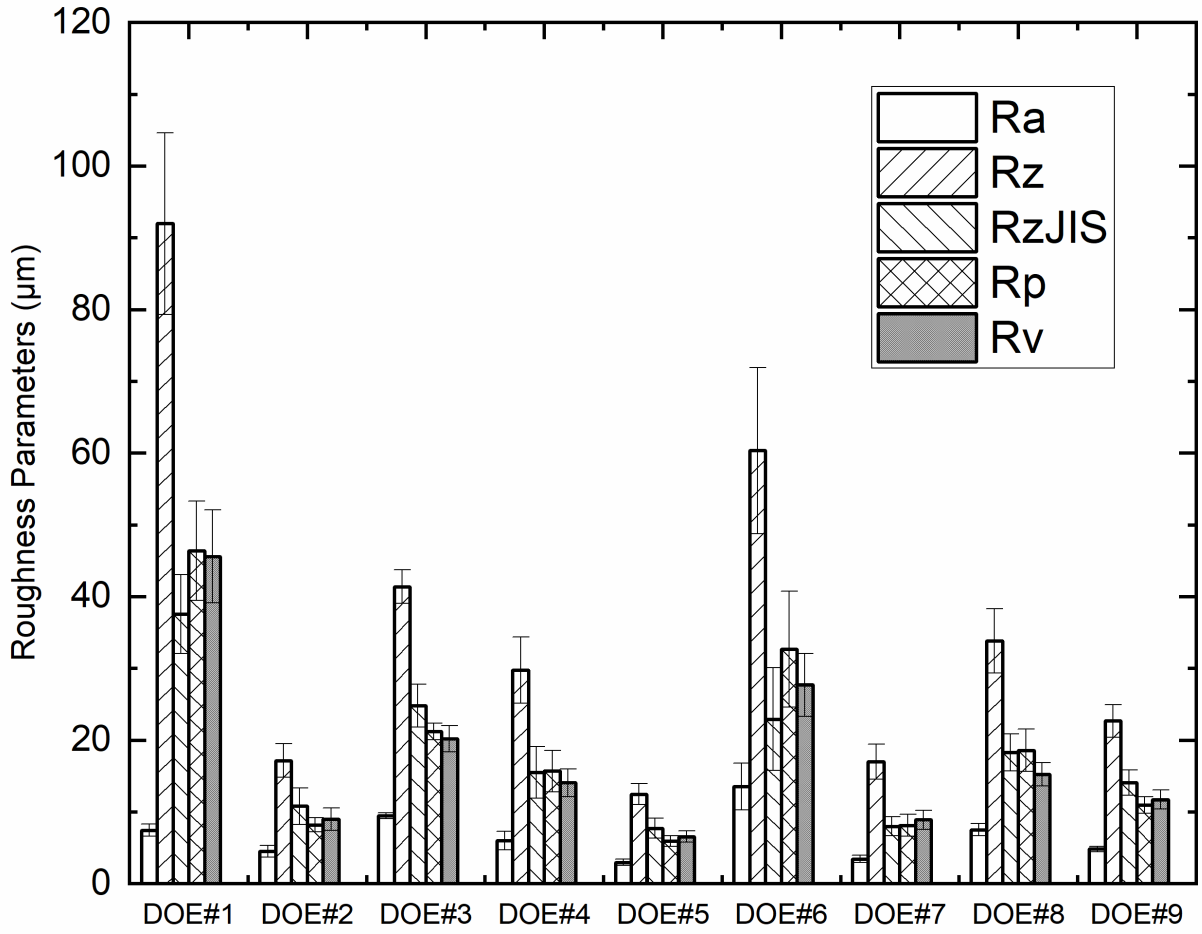

Fig 7. Bar chart representing the roughness for the nine experiments after nickel deposition.

nickel solution, as-built surface finish, alignment along the XY plane, and the optimal temperature.

The corresponding surface roughness measurements are as follows: Ra = 17.56 µm, Rz = 84.77 µm, RzJIS = 32.82 µm, Rp = 46.77 µm, Rv = 38.03 µm, Rc = 50.1 µm, Rt = 84.81 µm, and Rq = 21.0 µm (Fig.7).

Figure 6g corresponds to DOE#7, characterized by using a low phosphorus nickel solution, an electropolished surface finish, alignment along the XZ plane, and the optimal temperature setting. Surface roughness measurements for this particular configuration revealed the following values: Ra = 18.54 µm, Rz = 87.49 µm, RzJIS = 17.44 µm, Rp = 46.06 µm, Rv = 41.42 µm, Rc = 25.57 µm, Rt = 87.54 µm, and Rq = 22.22 µm. Figure 6h, emblematic of DOE#8, incorporates a set of parameters that entail a low phosphorus nickel solution, chempolished surface finish, alignment along the XY plane, and the temperature setting at the optimum level. The associated surface roughness characteristics are as follows: Ra = 17.44 µm, Rz = 71.88 µm, RzJIS = 20.65 µm, Rp = 32.87 µm, Rv = 39.01 µm, Rc = 55.84 µm, Rt = 71.9 µm, and Rq = 20.44 µm. Finally, Figure 6i represents DOE#9, wherein the experimental parameters encompass the utilization

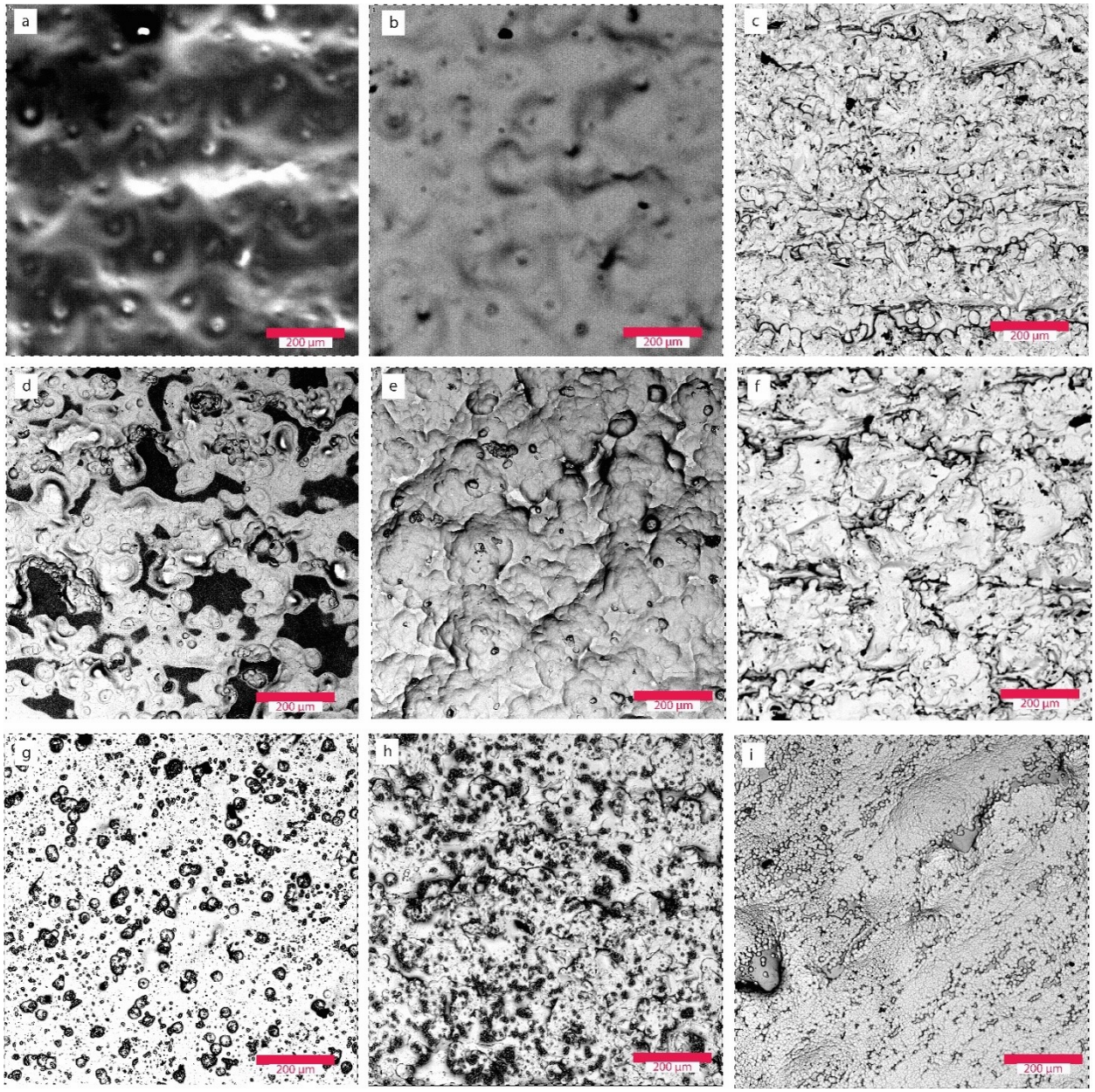

Fig 8. SEM imagery for (a) DOE#1, (b) DOE#2, (c) DOE#3, (d) DOE#4, (e) DOE#5, (f) DOE#6, (g) DOE#7, (h) DOE#7, (i) DOE#8, (j) DOE#9

of a low phosphorus nickel solution, an as-built surface finish, alignment along the YZ plane, and a temperature exceeding the optimum by 5°C. The surface roughness measurements for this configuration resulted in the following values: Ra = 11.30 µm, Rz = 51.26 µm, RzJIS = 19.56 µm, Rp = 26.08 µm, Rv = 25.17 µm, Rc = 25.49 µm, Rt = 51.26 µm, and Rq = 13.66 µm (Fig.7).

3.3 Scanning electron microscope (SEM)

In high phosphorous solution (Figures 8a-c) an approximate phosphorus concentration of up to 11% per deposition is observed. The primary objective of the coating is to maintain an amorphous structure characterized by the absence of grain boundaries or phase boundaries, effectively mitigating the creation of initiation sites for corrosion. The mid-phosphorous solution (Figures 8d,8e, and 8f) provides evidence of robust adhesion and elevated plating hardness in the context of deposition on an as-built sample. Elemental analysis performed on the sample surface reveals an approximate phosphorus concentration of around 8% per deposition. Notably, the low phosphorous solution (Figures 8g-i), in certain instances, observations indicate a phosphorus concentration of less than 5%, coupled with an inconsistent distribution pattern.

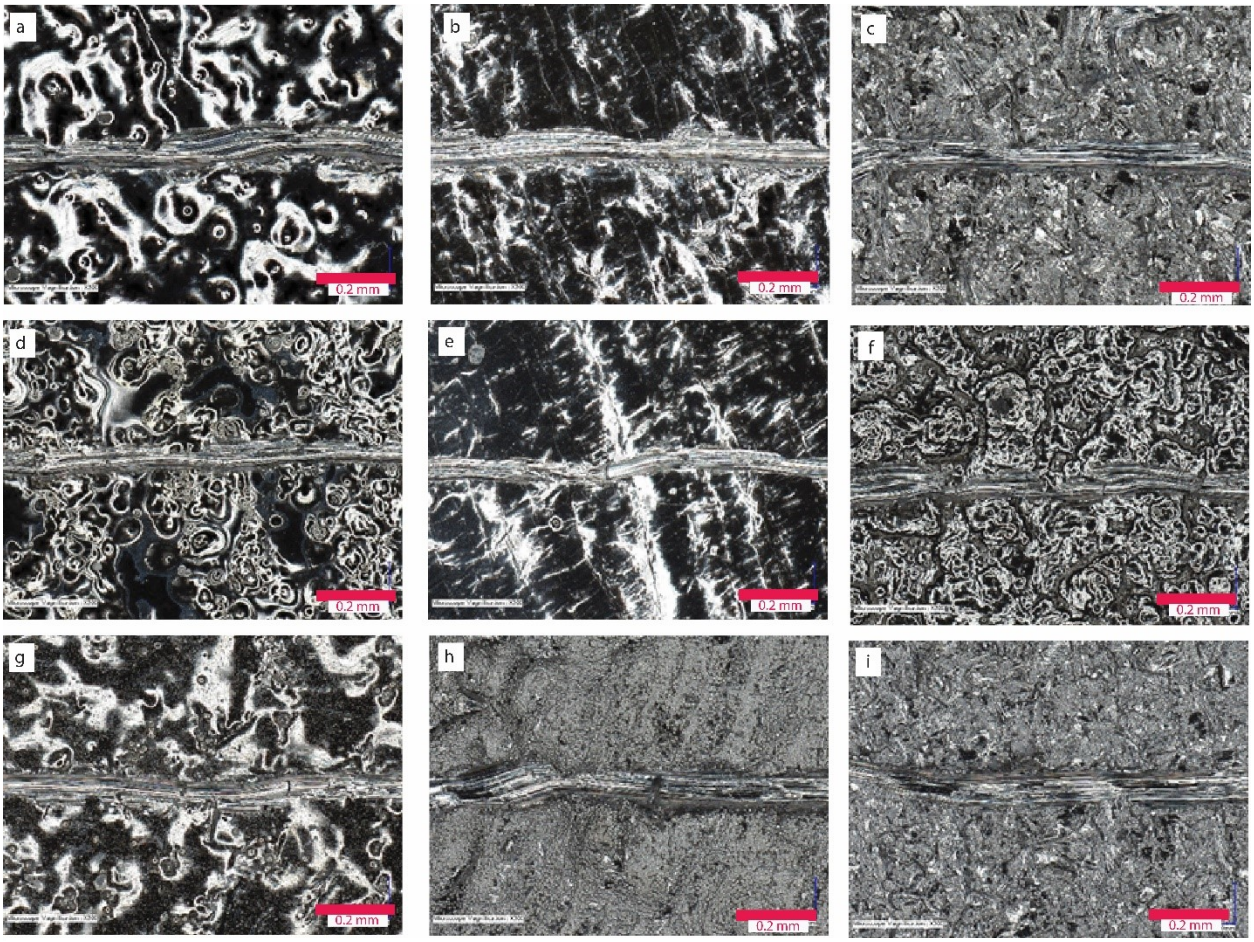

Fig 9. Scratch microscopy imagery for (a) DOE#1, (b) DOE#2, (c) DOE#3, (d) DOE#4, (e) DOE#5, (f) DOE#6, (g) DOE#7, (h) DOE#7, (i) DOE#8, (j) DOE#9

3.4 Scratch testing

Scratch testing is a fundamental technique for the comprehensive analysis and characterization of mechanical wear behaviors. The meticulous application of precisely defined scratches, performed in a consistent and reproducible fashion, becomes of paramount importance in the pursuit of surface wear resistance characterization. In the scope of our study, we opted for the standard 10 N scratch test methodology, conducted on samples coated with nickel (Fig. 9). Each of the nine samples (Table 3) was

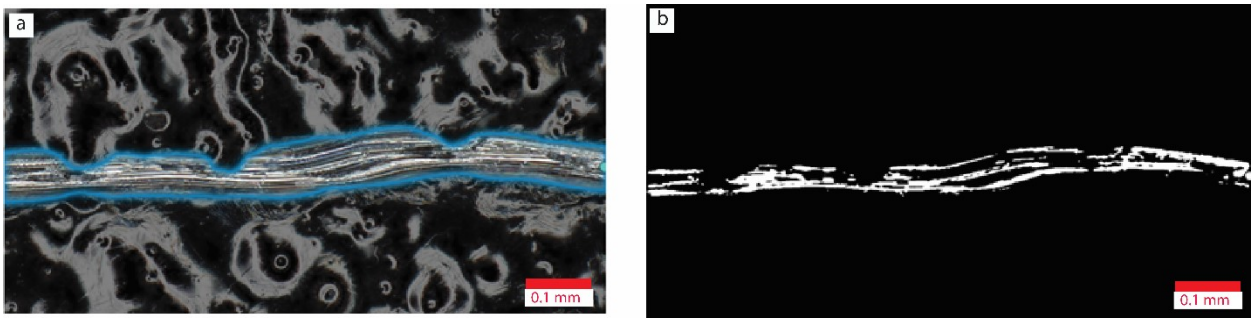

Fig. 10. (a) scratch image from SAM model (b) image after denoise and threshold

subjected to scratch testing (Fig. 9a-f). We were successful in obtaining clear scratch on nickel-coated samples with high phosphorous content (Fig. 9a-c), medium phosphorous content (Fig. 9d-f), and low phosphorous content (Fig. 9g-i). However, a major challenge was in analyzing different scratches. The

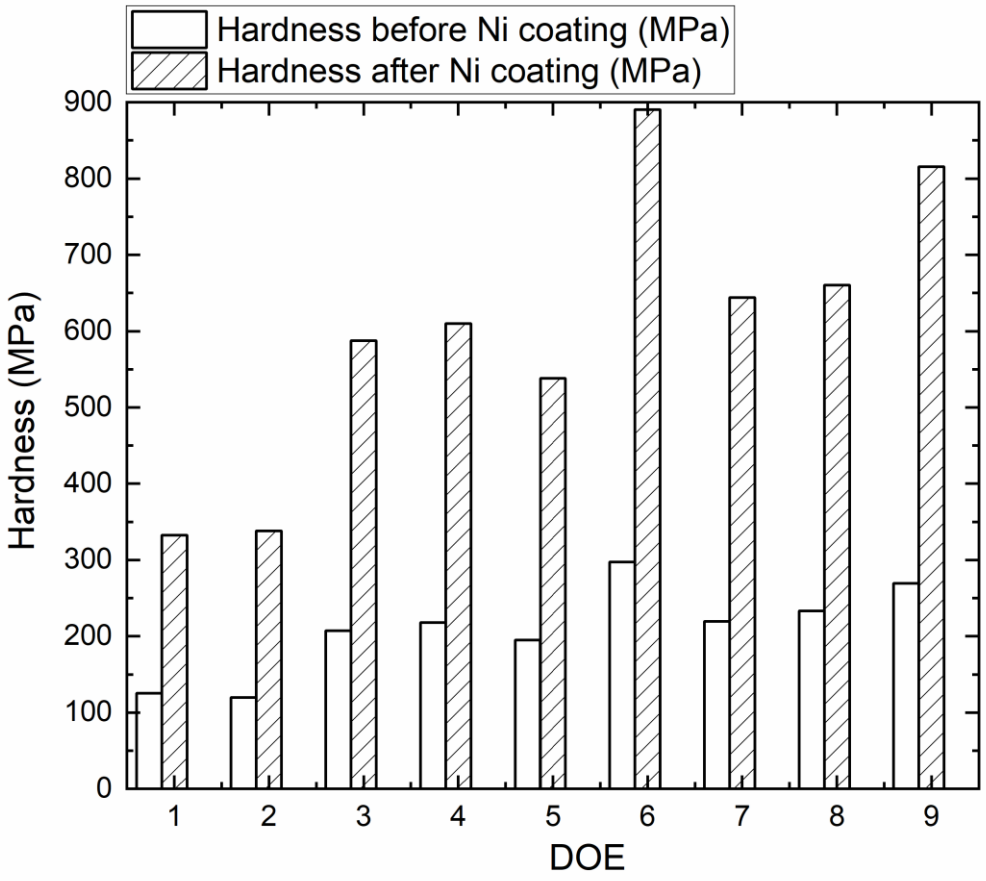

Fig. 11. Bar profile representing the roughness for the nine experiments after nickel deposition

acquisition of precise measurements of the scratch width from the microscopic imagery was difficult due

to the scratch's inconsistent width. Consequently, the methodology has been adapted to calculate the projected area of the scratch, which is then divided by its length to achieve a standardized measure (Fig. 10a). In the realm of image segmentation, the Segment Anything Model (SAM), developed by Meta, previously known as Facebook, has been employed. As a foundational model for segmentation, SAM has undergone training on a dataset encompassing 11 million images and in excess of one billion masks. The architecture of SAM is tripartite, consisting of an image encoder, a prompt encoder, and a mask decoder. The strength of SAM lies in its dual utility, offering both a no-code and a code-based solution. For the purposes of our experiment, the no-code, fully online option was selected. Subsequent to this, we applied denoising and thresholding processes using ImageJ to refine the results (example shown in Fig. 10b). Once we have performed instance segmentation and thresholding on the scratch, we proceed to determine the material's hardness using an equation (1) [45, 46].

$$Hs = 8P/\Pi w^2 \quad (1)$$

Where Hs = Scratch hardness number (MPa), P = Normal force (N), and w = scratch width in mm.

The presented data (Table 3) showcases the percentage increase in hardness across nine different Design of Experiments (DOE) trials. The results indicate a notable variation in the effectiveness of the treatments applied, with percentage increases ranging from 165.84% to 202.99%. The highest increase was observed in DOE trial 9 at 202.99%, while the lowest was in DOE trial 1 at 165.84%. This variability highlights the differing impacts of the experimental conditions on hardness. The overall trend suggests that the treatments applied in most DOE trials significantly enhance hardness, with several trials, such as DOE 6 and DOE 7, also demonstrating substantial improvements with increases of 199.46% and 193.16%, respectively.

Table 3. Surface Hardness before and after Ni coating

DOE	Hardness before Ni deposition	Hardness after Ni deposition	% Hardeness Increase
1	125.13	332.64	165.84
2	119.67	338.10	182.53
3	207.47	587.53	183.19
4	218.19	610.02	179.58
5	194.94	538.22	176.10
6	297.36	890.48	199.46
7	219.64	643.89	193.16
8	233.46	660.62	182.97
9	269.18	815.58	202.99

3.5 Taguchi Analysis:

Multi-plots serve as a visualization tool for elucidating the impacts of numerous factors on a response variable (Fig. 12). Within these plots; the presentation encompasses both the main effects and interaction effects of the factors on the response variable (Fig. 12). The main effects delineate the individual influence of each factor on the response variable, while the interaction effects depict the collective impact of two or more factors on the response variable. Surface finish impacted surface hardness significantly (Fig. 12b). electropolishing appears to yield low hardness compared to the chempolish and as-built samples. Interestingly, the phosphorus level significantly impacted the hardness level (Fig.12a). High phosphorous content appears to yield low hardness as compared to the medium and low phosphorous content. The

surface orientation and temperature factor's level impact was relatively weaker (Fig.1c,d). We also studied the strength of interaction between two parameters. All potential interactions between pairs of two factors are computed (Fig. 13.a). The interaction pairs are presented in descending order based on their Severity Index (SI), which is expressed on a scale from 0 to 100%. In cases involving interactions among pairs of factors with three levels, the Severity Index (SI) is indicative of the highest angle within the array of feasible combinations of line segments (Fig. 13.a). Interaction data shows the relative independence of a factor in relation to other factors. The highest interaction strength of 72.76 was observed between the orientation and temperature; it means changing orientation will necessitate an adjustment in the plating temperature for the desired results (Fig. 13a). On the other hand, a low severity index of 8.95 phosphorous and temperature interaction shows their independence from each other.

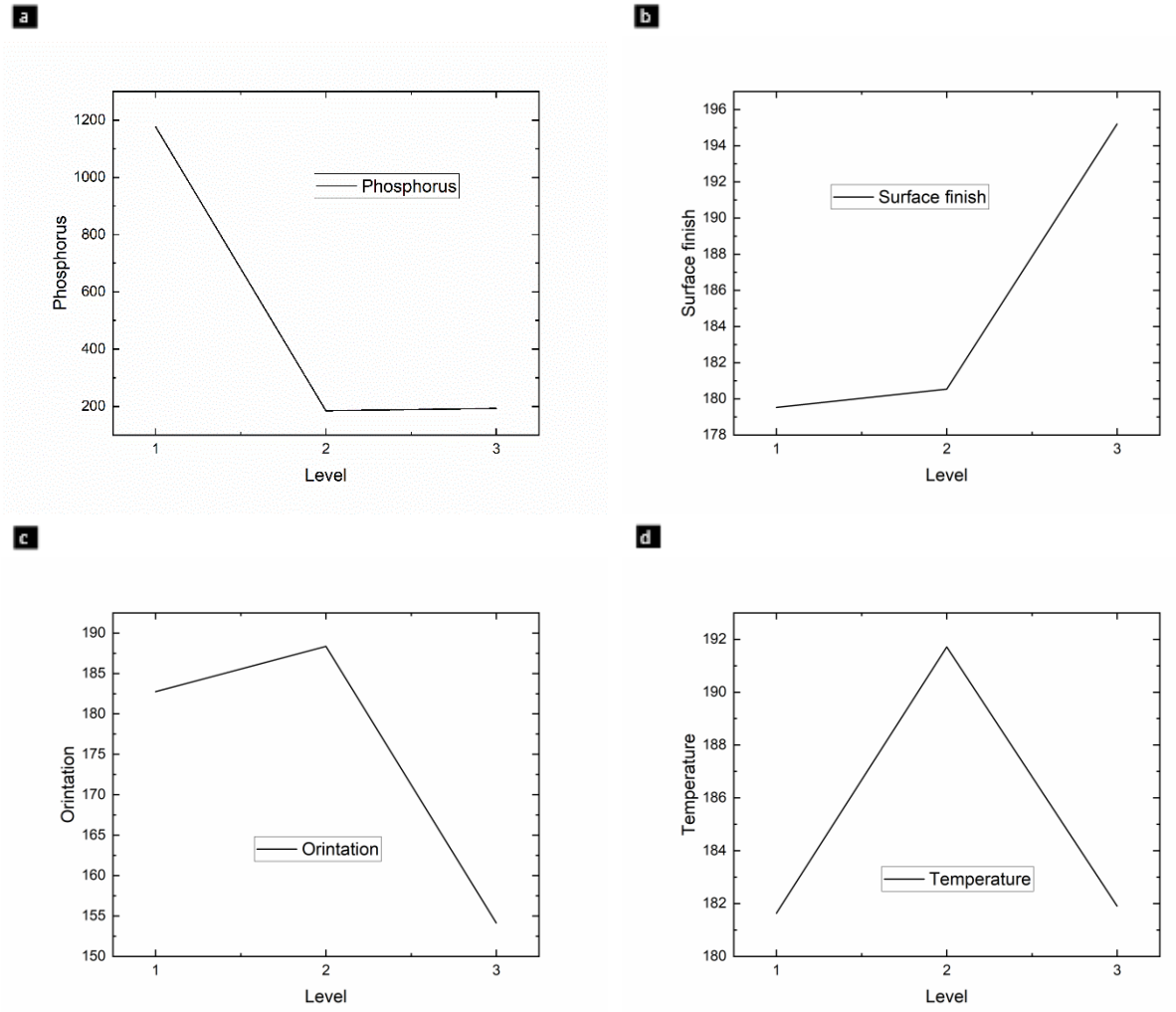

Fig 12. Taguchi Multi-plot analisys (a) phosphous (b) surface finish (c) Orientation (d) Temprature

We also investigated the impact of individual factors on film hardness (Fig. 13b). Phosphorus content and surface finish are the main factors in deciding the nickel coating hardness (Fig. 13b). This result is in line with the prior literature [47] relating the phosphorous content to the hardness of the nickel coating (Fig. 13b). Hardness is highest for the as-built surface. The reason is that high roughness enables the creation

of a better grip of the coating material on the surface (Fig. 13b). This result is consistent with the prior literature defining the impact of roughness on film adhesion.

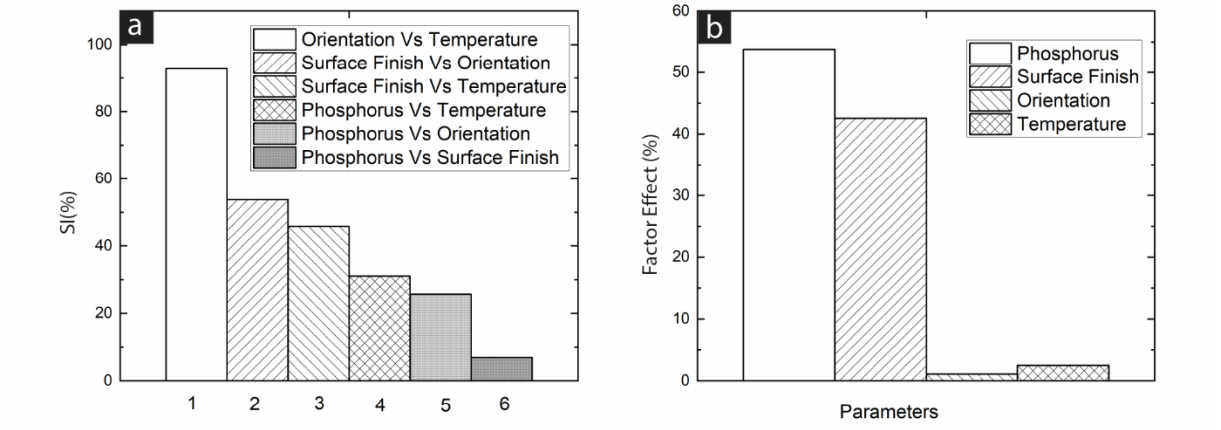

Fig. 13. Bar profiles showing (a) Interaction among factors (b) ANOVA analysis of impact of individual factors.

We also employed the Taguchi Design of experiment analysis to investigate the combination of parameters that will lead to the highest hardness. The optimal table represents the predictive equation delineating the anticipated performance under optimal conditions as well as any conceivable alternative conditions. The numerical values presented in the table are derived from computations conducted under the optimal condition, a state determined by the chosen quality characteristic for analysis. Conventional practice dictates the inclusion of only statistically significant factors (without pooling) in the computation of anticipated performance, aligning with established analytical methodologies. In the context of this experiment, The optimal condition for achieving the highest hardness is identified as a low-phosphorus nickel solution coupled with an as-built surface finish, YZ orientation, and a solution temperature of 90 degrees Celsius.

4. CONCLUSION

This study explores the utilization of electropolishing (EP) and chempolishing (CP) techniques for the removal of surface roughness, coupled with the subsequent application of electroless nickel plating as a protective layer coating on stainless-steel samples fabricated through additive manufacturing. These findings encapsulate the key outcomes of the investigation.

- The process of electropolishing exhibits a notable capability for achieving high-quality surface finishing, which is characterized by the rapid removal of material and giving a higher level of smoothness. In contrast, chempolishing emerges as a compelling alternative, primarily due to its capacity to remove material uniformly and impart smoothness to both internal and external surfaces. According to our Taguchi Design of Experiment, surface finishing was the main factor influencing the electroless nickel coating hardness

- Our study demonstrated that nickel-plated samples exhibited increased scratch resistance compared to their non-plated counterparts. Our observation is in line with prior work showing that electroless nickel indeed increases surface hardness.
- ANOVA analysis in our study suggested that surface orientation did not produce a significant effect on the hardness of the electroless nickel coating.
- As the main conclusion, it has been observed that the optimal combination yielding the highest surface hardness involves the utilization of a low-phosphorus nickel solution, along with a built surface finish, XY orientation, and a solution temperature of 90°C.
- In future studies, electroplishing followed by electroless nickel coating will be studied on samples with internal volumes. Further resaerch will also be needed to investigate the effect of applying the chempolishing and electropolishing sequentially on the AM components to prepare the AM surface for the electroless nickel coatings uniquely. Our recent work in this Journal demonstrated the unique microstructure and surface energy of AM components treated by chempolishing and electropolishing [36]. Hence, unique properties of electroless nickel coating may arise depending upon the specific sequence of the electropolishing and chempolishing.

Statements & Declarations

Funding

This research was funded by the National Science Foundation-CREST Award, grant number HRD- 1914751, Department of Energy/ National Nuclear Security Agency (DE-FOA-0003945), the Department of Energy's Kansas City National Security Campus. The Department of Energy's Kansas City National Security Campus is operated and managed by Honeywell Federal Manufacturing & Technologies, LLC, under contract number DE-NA0002839 and The NASA MUREP Institutional Research Opportunity Grant under Cooperative Agreement #80NSSC19M0196.

Competing Interests

Financial interests: Authors declare they have no financial interests

Author contributions

The conceptualization of the research idea is attributed to Pawan Tyagi. Experimental procedures were executed by Wondwosen, Dan, and Pablo. Subsequently, the composition of the manuscript fell under the responsibility of Wondwosen, with subsequent critical evaluation undertaken by both Pawan Tyagi and Kate Klein. Pawan Tyagi contributed experimental data pertinent to chemo-polishing and electropolishing procedures. Additionally, Lucas Rice facilitated the provision of experimental samples.

Data Availability: Data used in this paper will be made available upon reasonable request.

Reference

[1] E. Govekar, A. Jeromen, A. Kuznetsov, M. Kotar, and M. Kondo, "Annular laser beam based direct metal deposition," *Procedia Cirp,* vol. 74, pp. 222-227, 2018.

[2] J. Gardan, "Additive manufacturing technologies: state of the art and trends," *Additive Manufacturing Handbook,* pp. 149-168, 2017.

[3] D. Bourell and T. Wohlers, "Introduction to additive manufacturing," *Additive Manufacturing Processes,* vol. 24, pp. 3-10, 2020.
[4] I. Gibson, D. W. Rosen, B. Stucker, M. Khorasani, D. Rosen, B. Stucker*, et al.*, *Additive manufacturing technologies* vol. 17: Springer, 2021.
[5] K. S. Prakash, T. Nancharaih, and V. S. Rao, "Additive manufacturing techniques in manufacturing-an overview," *Materials Today: Proceedings,* vol. 5, pp. 3873-3882, 2018.
[6] A. Kumar, A. Choudhary, A. Tiwari, C. James, H. Kumar, P. K. Arora*, et al.*, "An investigation on wear characteristics of additive manufacturing materials," *Materials Today: Proceedings,* vol. 47, pp. 3654-3660, 2021.
[7] O. A. Mohamed, S. H. Masood, J. L. Bhowmik, and A. E. Somers, "Investigation on the tribological behavior and wear mechanism of parts processed by fused deposition additive manufacturing process," *Journal of Manufacturing Processes,* vol. 29, pp. 149-159, 2017.
[8] M. A. Melia, H.-D. A. Nguyen, J. M. Rodelas, and E. J. Schindelholz, "Corrosion properties of 304L stainless steel made by directed energy deposition additive manufacturing," *Corrosion Science,* vol. 152, pp. 20-30, 2019.
[9] C. Örnek, "Additive manufacturing–a general corrosion perspective," *Corrosion Engineering, Science and Technology,* vol. 53, pp. 531-535, 2018.
[10] G. Ko, W. Kim, K. Kwon, and T.-K. Lee, "The corrosion of stainless steel made by additive manufacturing: A review," *Metals,* vol. 11, p. 516, 2021.
[11] R. I. Revilla, M. Van Calster, M. Raes, G. Arroud, F. Andreatta, L. Pyl*, et al.*, "Microstructure and corrosion behavior of 316L stainless steel prepared using different additive manufacturing methods: A comparative study bringing insights into the impact of microstructure on their passivity," *Corrosion Science,* vol. 176, p. 108914, 2020.
[12] L. Huynh, J. Rotella, and M. D. Sangid, "Fatigue behavior of IN718 microtrusses produced via additive manufacturing," *Materials & Design,* vol. 105, pp. 278-289, 2016.
[13] J. Gockel, L. Sheridan, B. Koerper, and B. Whip, "The influence of additive manufacturing processing parameters on surface roughness and fatigue life," *International Journal of Fatigue,* vol. 124, pp. 380-388, 2019.
[14] A. Yadollahi and N. Shamsaei, "Additive manufacturing of fatigue resistant materials: Challenges and opportunities," *International Journal of Fatigue,* vol. 98, pp. 14-31, 2017.
[15] K. Carpenter and A. Tabei, "On residual stress development, prevention, and compensation in metal additive manufacturing," *Materials,* vol. 13, p. 255, 2020.
[16] B. A. Szost, S. Terzi, F. Martina, D. Boisselier, A. Prytuliak, T. Pirling*, et al.*, "A comparative study of additive manufacturing techniques: Residual stress and microstructural analysis of CLAD and WAAM printed Ti–6Al–4V components," *Materials & Design,* vol. 89, pp. 559-567, 2016.
[17] C. Li, Z. Liu, X. Fang, and Y. Guo, "Residual stress in metal additive manufacturing," *Procedia Cirp,* vol. 71, pp. 348-353, 2018.
[18] S. James and C. Dang, "Investigation of shear failure load in ultrasonic additive manufacturing of 3D CFRP/Ti structures," *Journal of Manufacturing Processes,* vol. 56, pp. 1317-1321, 2020.
[19] A. Hehr and M. J. Dapino, "Interfacial shear strength estimates of NiTi–Al matrix composites fabricated via ultrasonic additive manufacturing," *Composites Part B: Engineering,* vol. 77, pp. 199-208, 2015.
[20] D. Yavas, Z. Zhang, Q. Liu, and D. Wu, "Interlaminar shear behavior of continuous and short carbon fiber reinforced polymer composites fabricated by additive manufacturing," *Composites Part B: Engineering,* vol. 204, p. 108460, 2021.
[21] J. Chen, K. Bao, X. Zhang, Y. Cao, Y. Peng, J. Kong*, et al.*, "Adiabatic shear band development and following failure in 316L fabricated by an additive manufacturing process," *Materials Science and Engineering: A,* vol. 811, p. 141003, 2021.

[22] A. Biserova-Tahchieva, M. V. Biezma-Moraleda, N. Llorca-Isern, J. Gonzalez-Lavin, and P. Linhardt, "Additive Manufacturing Processes in Selected Corrosion Resistant Materials: A State of Knowledge Review," *Materials,* vol. 16, p. 1893, 2023.

[23] M. Megahed, H.-W. Mindt, N. N'Dri, H. Duan, and O. Desmaison, "Metal additive-manufacturing process and residual stress modeling," *Integrating Materials and Manufacturing Innovation,* vol. 5, pp. 61-93, 2016.

[24] S. Croll, "Surface roughness profile and its effect on coating adhesion and corrosion protection: A review," *Progress in Organic Coatings,* vol. 148, p. 105847, 2020.

[25] P. Tyagi, T. Goulet, C. Riso, R. Stephenson, N. Chuenprateep, J. Schlitzer*, et al.*, "Reducing the roughness of internal surface of an additive manufacturing produced 316 steel component by chempolishing and electropolishing," *Additive Manufacturing,* vol. 25, pp. 32-38, 2019.

[26] K. Technology. *8 Metal Surface Finishing Treatment Processes*. Available: https://www.kellertechnology.com/blog/8-common-types-of-surface-treatments-for-metal-parts/

[27] M. Donati, L. Kastnerova, N. Ptakova, M. Michal, and D. V. Kazakov, "Polypoid Atypical Spitz Tumor With a Fibrosclerotic Stroma, CLIP2-BRAF Fusion, and Homozygous Loss of 9p21," *Am J Dermatopathol,* vol. 42, pp. 204-207, Mar 2020.

[28] N. N. Kumbhar and A. Mulay, "Post processing methods used to improve surface finish of products which are manufactured by additive manufacturing technologies: a review," *Journal of The Institution of Engineers (India): Series C,* vol. 99, pp. 481-487, 2018.

[29] X. Peng, L. Kong, J. Y. H. Fuh, and H. Wang, "A review of post-processing technologies in additive manufacturing," *Journal of Manufacturing and Materials Processing,* vol. 5, p. 38, 2021.

[30] M. A. Mahmood, D. Chioibasu, A. Ur Rehman, S. Mihai, and A. C. Popescu, "Post-processing techniques to enhance the quality of metallic parts produced by additive manufacturing," *Metals,* vol. 12, p. 77, 2022.

[31] G. Yang, B. Wang, K. Tawfiq, H. Wei, S. Zhou, and G. Chen, "Electropolishing of surfaces: theory and applications," *Surface Engineering,* vol. 33, pp. 149-166, 2017.

[32] D. Landolt, "Fundamental aspects of electropolishing," *Electrochimica Acta,* vol. 32, pp. 1-11, 1987.

[33] S. E. Ziemniak, M. Hanson, and P. C. Sander, "Electropolishing effects on corrosion behavior of 304 stainless steel in high temperature, hydrogenated water," *Corrosion Science,* vol. 50, pp. 2465-2477, 2008.

[34] P. Tyagi, T. Goulet, C. Riso, and F. Garcia-Moreno, "Reducing surface roughness by chemical polishing of additively manufactured 3D printed 316 stainless steel components," *The International Journal of Advanced Manufacturing Technology,* vol. 100, pp. 2895-2900, 2019.

[35] W. Demisse, E. Mutunga, K. Klein, L. Rice, and P. Tyagi, "Surface finishing and electroless nickel plating of additively manufactured (am) metal components," in *ASME International Mechanical Engineering Congress and Exposition*, 2021, p. V02AT02A038.

[36] J. Dillard, A. Grizzle, W. Demisse, L. Rice, K. Klein, and P. Tyagi, "Alternating chempolishing and electropolishing for interior and exterior surface finishing of additively manufactured (AM) metal components," *The International Journal of Advanced Manufacturing Technology,* vol. 121, pp. 8159-8170, 2022.

[37] J. Bedmar, N. Abu-Warda, S. García-Rodríguez, B. Torres, and J. Rams, "Influence of the surface state on the corrosion behavior of the 316 L stainless steel manufactured by laser powder bed fusion," *Corrosion Science,* vol. 207, p. 110550, 2022.

[38] C. Loto, "Electroless nickel plating–a review," ed: Springer, 2016.

[39] F. Delaunois, V. Vitry, and L. Bonin, *Electroless nickel plating: fundamentals to applications*: CRC Press, 2019.

[40] J. Sudagar, J. Lian, and W. Sha, "Electroless nickel, alloy, composite and nano coatings–A critical review," *Journal of alloys and compounds,* vol. 571, pp. 183-204, 2013.
[41] G. O. Mallory and J. B. Hajdu, *Electroless plating: fundamentals and applications*: William Andrew, 1990.
[42] J. Hajdu and S. Zabrocky, "The future of electroless nickel," *Metal Finishing,* vol. 98, pp. 42-46, 2000.
[43] L. Wang, J. Li, and H. Liu, "A simple process for electroless plating nickel–phosphorus film on wood veneer," *Wood science and technology,* vol. 45, pp. 161-167, 2011.
[44] M. Kiguchi, "Surface modification and activation of wood," in *Chemical modification of lignocellulosic materials*, ed: Routledge, 2017, pp. 197-227.
[45] S. J. Bull and E. G. Berasetegui, "An overview of the potential of quantitative coating adhesion measurement by scratch testing," *Tribology International,* vol. 39, pp. 99-114, 2006/02/01/ 2006.
[46] A.-T. Akono and F.-J. Ulm, "An improved technique for characterizing the fracture toughness via scratch test experiments," *Wear,* vol. 313, pp. 117-124, 2014/05/15/ 2014.
[47] P. Sahoo and S. K. Das, "Tribology of electroless nickel coatings – A review," *Materials & Design,* vol. 32, pp. 1760-1775, 2011/04/01/ 2011.